Aerosol Science and Technology

ISSN: 0278-6826 (Print) 1521-7388 (Online) Journal homepage: www.tandfonline.com/journals/uast20

Estimating gas-particle partitioning in mixed emissions of plastic and biomass burning thermal degradation products

Emily Halpern, Dominick Dotson, Qiaorong Xie, Peter Christ, Killian MacFeely, Lauren Heirty, Sergey A. Nizkorodov & Alexander Laskin

To cite this article: Emily Halpern, Dominick Dotson, Qiaorong Xie, Peter Christ, Killian MacFeely, Lauren Heirty, Sergey A. Nizkorodov & Alexander Laskin (2026) Estimating gas-particle partitioning in mixed emissions of plastic and biomass burning thermal degradation products, Aerosol Science and Technology, 60:7, 797-811, DOI: 10.1080/02786826.2025.2609955

To link to this article: https://doi.org/10.1080/02786826.2025.2609955

AEROSOL SCIENCE AND TECHNOLOGY
2026, VOL. 60, NO. 7, 797–811
https://doi.org/10.1080/02786826.2025.2609955

Estimating gas-particle partitioning in mixed emissions of plastic and biomass burning thermal degradation products

Emily Halpern[a], Dominick Dotson[a], Qiaorong Xie[a], Peter Christ[a], Killian MacFeely[a], Lauren Heirty[a], Sergey A. Nizkorodov[b], and Alexander Laskin[a,c]

[a]Department of Chemistry, Purdue University, West Lafayette, Indiana, USA; [b]Department of Chemistry, University of California, Irvine, Irvine, California, USA; [c]Department of Earth Atmospheric and Planetary Sciences, Purdue University, West Lafayette, Indiana, USA

ABSTRACT

Wildfires at the wildland–urban interface (WUI) generate highly complex and poorly characterized mixtures of gas-phase and condensed-phase pollutants. As the frequency and severity of WUI events increase, evaluating gas–particle partitioning and mixing behavior of these emissions becomes essential for predicting their environmental impact. Experimental characterization of WUI aerosol emissions is particularly challenging due to the diversity of materials and variability in combustion conditions. Thus, practical methods for estimating chemical composition and gas–particle partitioning behavior of mixed-source emissions, with the potential to guide burning experiments with different fuel combinations, are valuable for assessing their atmospheric implications. Here, emission profiles resulting from the thermal degradation of selected plastic reference materials: polyethylene (PE), polypropylene (PP), polystyrene (PS), and polyvinyl chloride (PVC), are investigated using temperature-programmed desorption coupled with direct analysis in real time ionization source and high-resolution mass spectrometry. Combined with established parameterization methods, these measurements enable the construction of VBS distributions for the thermal decomposition products of individual plastics. Plastic-specific VBS distributions are then numerically combined with previously reported biomass burning aerosol properties to evaluate gas-particle partitioning and aerosol-phase viscosity in mixed emissions. Calculations indicate that emissions from PE and PP burning have greater potential to lower volatility and increase particle-phase viscosity in mixed WUI plumes compared to PS and PVC. These emissions may lead to an estimated 20% increase in particle-phase organic mass and induce viscosity changes.

GRAPHICAL ABSTRACT

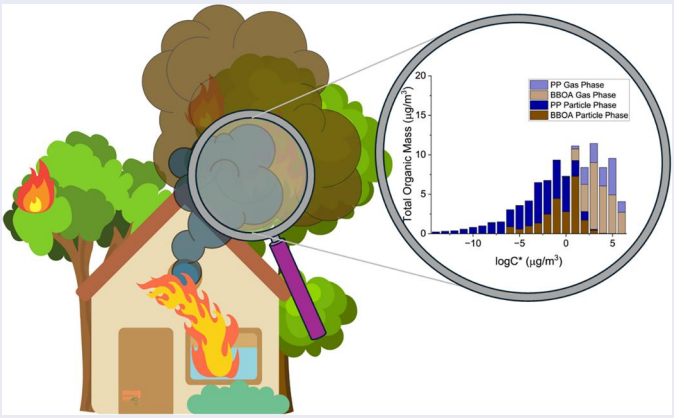

ARTICLE HISTORY
Received 8 August 2025
Accepted 13 December 2025

EDITOR
Chia Chen Wang

CONTACT Alexander Laskin alaskin@purdue.edu Department of Chemistry, Purdue University, West Lafayette, IN, 47907, USA.

Supplemental data for this article can be accessed online at https://doi.org/10.1080/02786826.2025.2609955.

Introduction

Biomass burning organic aerosol (BBOA), emitted from wildfires and agricultural burns, consists of complex mixtures of organic compounds (Laskin et al. 2015, Laskin et al. 2025). These light-absorbing particles influence atmospheric radiation balance, contribute to degraded air quality, and impact human health (Burke et al. 2023; Chakrabarty et al. 2023; Fang et al. 2023). Exposure to BBOA has been associated with oxidative stress and increased risks of cardiovascular, neurological, and respiratory diseases (Jaffe et al. 2020; Benedict et al. 2024; Fang et al. 2025). The hazards posed by BBOA from wildfires are of particular concern, as the frequency and severity of wildfire events have been increasing in response to shifts in environmental conditions and land management practices (Balch et al. 2017; Ganteaume et al. 2021). Additionally, BBOA can be transported over long distances, reaching regions thousands of kilometers from the source and affecting communities far from the emission's origin (Jaffe et al. 2020; Benedict et al. 2024).

The wildland-urban interface (WUI) is an area where residential and commercial developments are mixed with or adjacent to undeveloped natural landscapes (Hammer et al. 2009). Despite their growing relevance, WUI emissions remain understudied relative to wildfires in purely vegetated regions, largely because of the increased complexity associated with burning mixed materials (Benedict et al. 2024; Hopstock et al. 2024). The expansion of WUI areas further elevates the likelihood of fire ignition and spread in these regions (Balch et al. 2017; Ganteaume et al. 2021). Humans also start approximately 84% of wildfires, resulting in increased WUI fire frequency. Many recent WUI events, such as those in the Los Angeles area in 2025, have been particularly destructive. Wildfires occurring in the WUI produce particularly complex emissions of gas-phase species and aerosol mixtures compared to vegetation-only fires, as a result of the burning of commercial materials such as plywood, plastic, insulation, and other structural components (Ganteaume et al. 2021; Holder et al. 2023). These mixed-source emissions also influence the regional gas-particle partitioning behavior of airborne pollutants, thereby affecting the atmospheric transport, chemical reactivity, and air quality impacts of the resulting aerosols (Liang et al. 2023).

Plastic materials constitute a substantial fraction of residential and commercial infrastructure, accounting for 10–25% of building content. Common applications of plastic in buildings include insulation, furniture, flooring, carpeting, and piping, comprising a diverse array of polymers such as polyethylene, polyurethane, polypropylene, polyvinyl chloride, polytetrafluoroethylene, polystyrene, and nylon (National Academies of Sciences, Engineering, and Medicine et al. 2022). When subjected to high temperatures, plastics generate highly complex emissions that can cause significant environmental and health hazards (Zhang et al. 2023; National Academies of Sciences, Engineering, and Medicine et al. 2022). These emissions have also been shown to induce high oxidative stress and cytotoxicity (Wu et al. 2021; Bardales Cruz et al. 2023), containing a variety of toxic constituents, including halogenic acids, PAHs, dioxins, furans, olefins, paraffins, plasticizers, and other additives (Holder et al. 2023; Zhang et al. 2023). Plastic burning also typically results in high concentrations of fine particulate matter, with emissions also enriched in volatile organic compounds (VOCs) that facilitate secondary organic aerosol (SOA) formation (Bardales Cruz et al. 2023; Hopstock et al. 2024). Plastic burning particulate matter has been identified as a source of environmentally persistent free radicals (EPFRs) (Salim et al. 2025). The compositional variability complicates experimental evaluation of plastic burning emissions, rendering a comprehensive assessment both resource-intensive and analytically challenging (Hoffer et al. 2020). In WUI fires, plastics are typically co-burnt with biomass, leading to complex compositions that alter aerosol volatility, reactivity, and viscosity. These mixed-source emissions further complicate efforts to characterize the composition, physical properties, and environmental impacts of WUI-derived aerosols.

To assess the impact of WUI emissions on human health and the environment, improved characterization of aerosols formed from mixed-emission sources is essential. However, the wide variety of materials present in WUI fires makes comprehensive experimental measurements of all potential mixtures both challenging and time-consuming. Plastic waste materials have previously been characterized using temperature-programmed desorption (TPD) coupled with direct analysis in real-time (DART) ionization and high-resolution mass spectrometry (HRMS) (Zhang et al. 2020; Forbes et al. 2023; Halpern et al. 2025). The TPD step of this platform enables controlled thermal decomposition of plastic samples, followed by the evaporation of their thermal decomposition products, which mimic plastic thermal degradation processes. Similarly, the composition and volatility of BBOA components have been experimentally assessed using the same technique, as described by Xie et al. 2024a. In this study, a practical framework is presented that integrates TPD-DART-

HRMS measurements with established volatility basis set (VBS) parameterizations (Donahue et al. 2011, 2012; Murphy et al. 2012) to model the gas-particle partitioning behavior of organic aerosols composed of mixed species originating from plastic and biomass sources. This approach facilitates the initial evaluation of source-specific emission characteristics and atmospheric transformation trends associated with organic aerosols from WUI fires involving chemically diverse materials.

Methods

Polyethylene (PE, low-density), polypropylene (PP, average MW 12,000 Da), polystyrene (PS, average MW 35,000 Da), and polyvinyl chloride (PVC, low molecular weight), purchased from Sigma-Aldrich (St. Louis, MO), were used in this study as reference plastic materials. These representative polymers were selected based on their widespread use in household products and construction materials commonly found in the WUI regions (National Academies of Sciences, Engineering, and Medicine et al. 2022) and their previously documented potential to produce multi-component thermal decomposition emissions (Halpern et al. 2025). Figure 1 illustrates the experimental setup. Approximately 1 mg of each plastic sample cut from a larger piece was placed onto a copper substrate for TPD-DART-HRMS analysis. The copper substrate was positioned on an Ion-Rocket™ heating stage (BioChromato Inc., Fujisawa, Kanagawa, Japan) connected to a DART ionization source (JumpShot®, IonSense Inc., Saugus, MA, USA) and interfaced with an Orbitrap Q Exactive HF-X high-resolution mass analyzer (Thermo Scientific Inc.). The heating protocol involved an initial hold at 50 °C for 0.5 min, followed by a temperature ramp of 100 °C min^{-1} until reaching 600 °C, which was then maintained for 1 min. A glass T-shaped connector was employed to direct evaporating analyte into the flow of ionizing gas. The DART ionizing gas stream, carrying metastable excited-state helium (He*) and associated secondary ionizing species, was maintained at 200 °C with a flow rate of 2 L/min. After each experiment, no visible plastic residue or char remained in the copper substrate. However, a light visible condensate was occasionally observed on the inner surface of the T-shaped glass connector. To prevent cross-contamination, the connector was thoroughly cleaned between runs, and a new copper substrate was used for every experiment.

The ion abundances observed in positive ion mode for all plastic samples analyzed in this study were significantly higher than those detected in negative mode, with enhancements of approximately two-fold for PE, three-fold for PP, and ten-fold for PS (Figure S1) for the entire thermogram. These substantially higher signal intensities are attributed to the enhanced ionization efficiency of hydrocarbon species under positive-mode DART ionization (Chernetsova et al. 2011). In the case of PVC, all ions detected in negative mode were $Cu_xCl_{x+1}^-$ ($x = 1$–7) species formed through reactions between HCl thermal decomposition products and the copper substrate, with no hydrocarbon products observed (Halpern et al. 2025). Consequently, the composition and properties of plastic thermal decomposition products are discussed based on TPD-(+)DART results, while TPD-(−)DART results are provided in the online supplementary information.

The mass spectrometer was operated at a mass resolving power of $m/\Delta m = 240{,}000$ at m/z 200, with data acquisition in m/z 100–1000 range. The elemental composition of plastic thermal decomposition products was determined from the assignments of HRMS features integrated over the full heating range from 50 °C to 600 °C (Figure 1b). Individual HRMS peaks were extracted using DeconTools Autoprocessor (http://omics.pnl.gov/software/) (Jaitly et al. 2009). Molecular formulas were assigned using MIDAS (version 1.1) molecular formula calculator developed by the National High Magnetic Field Laboratory, USA, assisted by Kendrick mass defect (KMD) analysis and grouping. HRMS were grouped in two-dimensional CH_2-H_2 KMD groups using custom Excel macros developed for background subtraction and KMD classification (Hughey et al. 2001; Roach et al. 2011). Formula assignments were constrained by a mass tolerance of ±2 ppm and limited to the following elemental composition ranges: $C \leq 100$, $H \leq 200$, $N \leq 1$, and $O \leq 50$. Ion species were restricted to $[M+H]^+$, $[M+NH_4]^+$, and $[M^\bullet]^+$ ions in positive mode and $[M\text{-}H]^-$, $[M+NO_2]^-$, $[M^\bullet]^-$ ions in negative mode. In the case of PVC, abundant $[Cu_xCl_{x+1}]^-$ cluster ions were observed in negative mode. Additionally, a small number of chlorinated organic species were detected in positive mode, although their total ion signal was minimal (~0.5% of the total). However, molecular metrics, gas-particle partitioning, and viscosity cannot be determined for these materials, so estimates were not compiled for (—)DART PVC measurements.

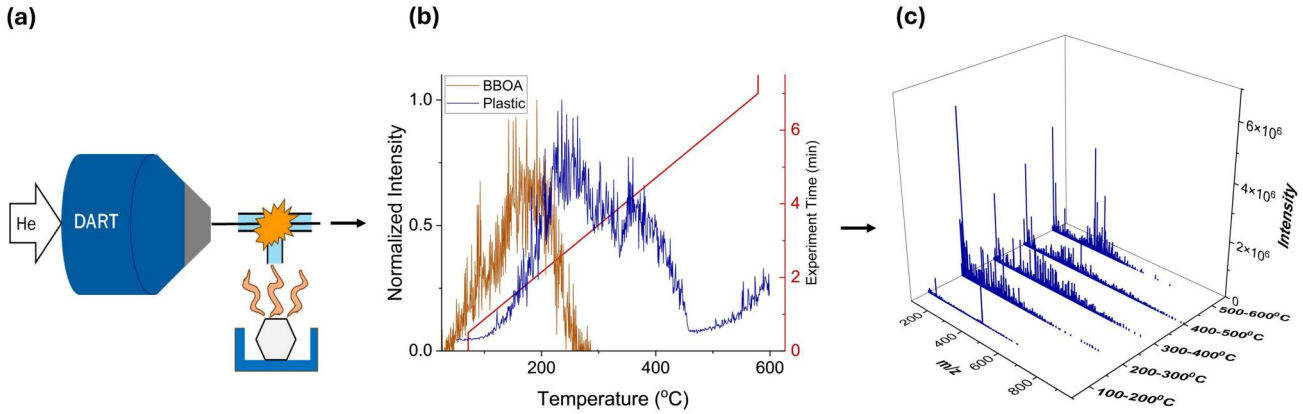

Figure 1. Schematic overview of the TPD-DART-HRMS experiments for the characterization of plastic thermal decomposition products. (a) Plastic samples are placed onto a copper substrate and subjected to controlled heating to induce thermal decomposition. The resulting products evaporate and are subsequently ionized in the DART gas stream by metastable helium (He*) and associated secondary gas-phase ionization mechanisms. (b) Representative (—)DART thermograms of a polypropylene (PP) sample and a biomass burning organic aerosol (BBOA) sample reported in previous studies, (Xie et al. 2024a) highlighting the higher temperature range of PP decomposition products compared to the lower-temperature evaporation of BBOA components. The red line indicated the heating ramp of the TPD-DART source. (c) Mass spectra of PP thermal decomposition products recorded across different temperature intervals, showing molecular features characteristic of plastic thermal decomposition emissions.

Based on the ion formula assignments, a series of molecular metrics was calculated for the corresponding neutral molecular species (M) representing plastic thermal decomposition products. In these calculations, n_C, n_H, and n_O represent the number of carbon, hydrogen, and oxygen atoms in each molecule (M), respectively. Since none of the analyzed plastic types contain nitrogen in their polymer backbones, all nitrogen-containing assignments were interpreted as adduct ions $[M+NH_4]^+$ in positive mode and $[M+NO_2]^-$ in negative mode, consistent with previous observations using the DART ion source (Gross 2014) The double bond equivalent (DBE) values were calculated using Equation (1) (Meija 2006):

$$DBE = n_C - \frac{n_H}{2} + 1 \quad (1)$$

The aromaticity index (AI_{mod}) values were calculated using Equation (2) (Koch and Dittmar 2006):

$$AI_{mod} = \frac{1 + n_C - 0.5 * n_O - 0.5 * n_H}{n_C - 0.5 * n_O} \quad (2)$$

The carbon oxidation state (OS_c) values were calculated using Equation (3) (Kroll et al. 2011):

$$OS_C = 2 * \frac{n_O}{n_C} - \frac{n_H}{n_C} \quad (3)$$

Results and discussion

Methodology for assessing the volatility and gas-particle partitioning of plastic thermal decomposition product mixtures. The DBE, AI_{mod}, and OS_C plots of the thermal decomposition products of each plastic type for (+/−) DART are shown in Figures S2–S4 (Supplemental Note 1). DBE values falling between the linear polyene line and planar aromatic limit depicted in Figure S2 will likely contribute to the pool of light-absorbing species in the atmosphere. In general, the range of DBE values for plastic thermal decomposition products depends on the plastic type. Both PE and PP produce long aliphatic chains with mostly non-light-absorbing products when thermally decomposed, while PS and PVC produce both aliphatic chains and aromatic molecules, which could be light-absorbing. The aromatic products from PS degradation result from thermally stable benzene moieties comprising the original polymer backbone, while smaller, alkane organic species are also produced in varying amounts depending on the efficiency of thermal decomposition (Gonçalves et al. 2008). In contrast, aromatic species products from PVC degradation are formed during the thermal decomposition processes, facilitated by the elimination of HCl and free radical chemistry, producing polyaromatic hydrocarbons (PAHs) (Huang et al. 2018). The AI_{mod} plots in Figure S3 depict the wide range of aromaticity for plastic products. All four plastics produce condensed aromatic species (AI_{mod}>0.67), in low quantities, as well as species with no aromatic character. The oxidation state of carbon (OS_c) in detected thermal decomposition plastic products is in the range between −2 and 0, as depicted in Figure S4. These species are mostly reduced and have low oxygen contribution, similar to the OS_c ranges of hydrocarbon-

like primary organic aerosol and biomass burning organic aerosol (Kroll et al. 2011).

In the TPD-DART-HRMS experiments, mass spectra are continuously recorded, allowing for sensitive detection and characterization of the evolving emission profiles from plastic samples during temperature-controlled thermal decomposition, as illustrated in Figure 1. For relatively small molecular species, such as those that dominate BBOA, apparent enthalpies of sublimation/evaporation for individual species can be determined through quantitative analysis of the thermograms (West et al. 2023; Xie et al. 2024a). However, as shown in the (−)DART thermograms of plastic and BBOA in Figure 1b, the characteristic thermograms of plastic products peak at significantly higher temperatures, reflecting a combination of both thermal decomposition of the starting plastic material and subsequent volatilization of the products. Consequently, the enthalpies of sublimation/evaporation of plastic-derived thermal decomposition products cannot be directly inferred from thermograms alone, necessitating the alternative estimation approach described below.

As plastics undergo thermal decomposition, their degradation products are released into the gas phase, where they can subsequently condense to form aerosol particles. Figure 2 provides a conceptual overview of the equilibrium partitioning of these products between the gas and particle phases, along with a summary of the component-specific data processing methods employed in this study. This partitioning behavior is governed by the volatility of individual species and key external environmental factors, including temperature, pressure, and the total particulate organic mass loading in the system. The elemental compositions of the detected thermal decomposition products are determined through the assignment of HRMS ion features, assuming complete formation of gas-phase species, with appropriate corrections applied for their ionization forms. These assignments allow for the calculation of molecular weights for the corresponding neutral species. The mass fractions (f_i) of the individual species are then calculated using Equation (4):

$$f_i = \frac{\sigma_i \times h_i \times MW_i}{\sum_i \sigma_i \times h_i \times MW_i} \quad where \sum_i f_i = 1 \qquad (4)$$

Here, MW_i is the molecular weight of the detected neutral species (i); h_i represents the integrated area of the single ion thermogram (SIT) corresponding to its characteristic parent ion; σ_i is a sensitivity correction factor (defined here as the inverse of the ionization sensitivity) that accounts for the relative ionization efficiency of each species.

While the ionization mechanism of DART is multifaceted and involves complex gas-phase ion chemistry, its fundamental processes can be summarized as follows. Excited metastable helium atoms (He*) are generated *via* glow discharge inside the ionization source and directed into the T-shaped glass junction, where they collide with gas-phase analyte molecules (M) desorbed from the heated substrate (Figure 1a). The 19.8 eV energy of He* enables efficient ionization of ambient nitrogen (N_2) and most organic molecules through Penning ionization ($M + He^* \rightarrow M^{\bullet+} + He + e^-$). Ambient water vapor is also ionized, forming protonated water clusters, $H_3O^+(H_2O)_n$, which facilitate secondary proton transfer reactions, resulting in the formation of $[M+H]^+$ ions. In the presence of trace ammonia, NH_4^+ ions may also form, yielding $[M+NH_4]^+$ adducts. Electrons released through Penning ionization are captured by atmospheric oxygen, generating superoxide anions $O_2^{\bullet-}$, which then engage in further ion–molecule reactions leading to the formation of deprotonated species $[M\text{-}H]^-$ (Gross 2014). Importantly, the TPD-DART experimental setup decouples analyte desorption from ionization, allowing the ionization efficiency to be governed primarily by bimolecular gas-phase reaction kinetics between the analyte molecules (M) and He* reagent supplied in large excess. As the analyte is gradually desorbed at relatively low concentrations, the ionization process remains in a kinetic regime controlled by He* and analyte collisions. Under these conditions, DART ionization is stable and reproducible (West et al. 2023; Xie et al. 2024b, 2024a, 2025). In this scenario, assuming low contribution from other kinetic schemes as is implied by previous studies and literature (Gross 2014), the approximate sensitivity correction factors (σ_i) for individual species can be inferred from differences in their estimated He* and analyte collision cross sections.

Details on the evaluation of sensitivity correction factors (σ_i) based on calculated collision cross sections (CCS) for representative analyte molecules are provided in Supplementary Note 2. Briefly, we selected monomerically related products, consisting of structurally similar homologous species that reflect the original polymer backbone with progressively increasing carbon chain length. The molecular geometries of these compounds were optimized using density functional theory (DFT) with the B3LYP functional and the 6–31 G* basis using the 'Q-Chem 5′ program package, enabling estimation of their gas-phase CCS

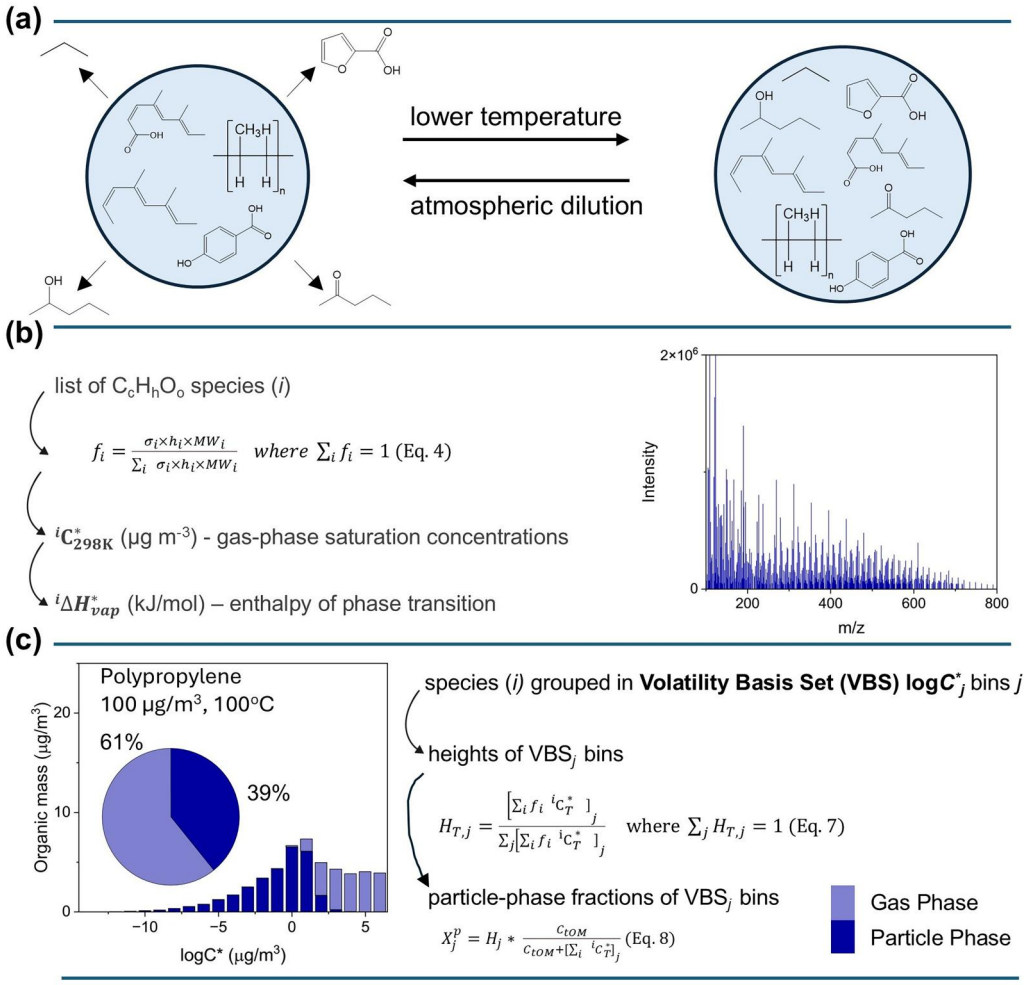

Figure 2. Schematic summary of the workflow used to estimate the volatility and gas-particle partitioning behavior of plastic thermal decomposition product mixtures. Each of the sequential steps noted in this caption are further elaborated in the manuscript text. (a) Graphic representation of the equilibrium partitioning of plastic thermal decomposition products between gas and particle phases, as governed by temperature (T, K) and total organic mass loading in air (C_{tOM}, μg·m^{-3}). (b) Identification of individual plastic thermal decomposition products (*i*), illustrated by the mass spectrum obtained for PP. Saturation vapor pressures ($^{i}C^{*}_{298,}$ μg·m^{-3}) are calculated using methods described in Supplemental Note 3. The corresponding apparent enthalpies ($^{i}\Delta H^{*}$, kJ mol^{-1}) associated with the condensed-to-gas phase transitions are determined using the limit II parameterization reported by Ranjan et al. (2012). (c) Construction of volatility basis set (VBS) distributions for plastic pyrolysis mixtures, exemplified by the VBS distribution of PP products at $T = 100\,°C$ and $C_{tOM} = 100\,\mu g\ m^{-3}$. The light blue indicates the gas-phase fraction, while the dark blue represents the particle-phase fraction.

values (Figure S5, Table S1) (Epifanovsky et al. 2021). CCS values were determined from the Ion Mobility Spectrometry Suite for each representative molecule (IMoS; https://www.imospedia.com/imos/) based on the projected area approximation method. (Shrivastav et al. 2017) The resulting CCS values were used to construct plots of the dimensionless ratio R_{MWi}=CCS$_{MWi}$/CCS$_{100}$ versus MW, as shown in Figure S6. Here, CCS$_{100}$ represents the reference value derived from a linear regression fit to the dataset ($R = a \times MW_i + b$) normalized such that R_{100}=1. These R ratios provide a standardized framework for comparing the CCS values of individual species as a function of molecular weights. Due to the similarity of the R_{MWi} ratios among the thermal decomposition products of PE, PP, and PVC, a single regression line was derived for the products from these three plastic types. A separate regression line was determined for PS products due to their distinct aromatic moieties. Sensitivity correction factors (σ_i) were then calculated using Equation (5):

$$\sigma_i = \frac{1}{(a \times MW_i + b)} \tag{5}$$

While these σ_i values do not capture the fundamental kinetics of the various ionization reactions occurring in DART, they provide a first-order approximation of the generally higher ionization

efficiencies associated with larger products possessing greater collision cross sections.

The initial reference volatility values of individual species, expressed as gas-phase saturation mass concentrations at 298 K ($^{i}C^{0}_{298K}$, μg·m^{-3}), were calculated from their elemental formulas using the "Molecular Corridors (MC)" parameterization by Li et al. (2016). These $^{i}C^{0}_{298K}$ values were then refined to yield corrected $^{i}C^{*}_{298K}$ values by applying a correction factor derived from comparisons between MC-predicted volatilities and experimental data reported for laboratory-generated secondary organic aerosol (SOA) (West et al. 2023), as illustrated in Figure S7. The detailed calculation procedures for these volatility estimates are provided in Supplemental Note 3. Results of the $^{i}C^{*}_{298K}$ estimates for each of the plastic types are provided in Figure S8.

Calculation of the temperature-dependent gas-phase saturation mass concentrations of individual species ($^{i}C^{*}_{T,}$ μg·m^{-3}) requires additional estimates of the apparent enthalpies ($^{i}\Delta H^{*}$, kJ mol^{-1}) associated with their transition from the condensed to gas phase. These ΔH^{*} values can be calculated using existing parameterizations of ΔH^{*} as a function of $\log C^{*}_{298K}$, which have been reported for various organic aerosol mixtures. Our recent field study demonstrated that pairs of $^{i}\Delta H^{*}$ and $^{i}C^{*}_{298K}$ values reported for components of ambient aerosol mixtures generally fall within the bounds of two previously reported parameterization lines: limit I defined by $\Delta H^{*} = -11 \times \log(C^{*}_{298K}) + 129$ (Epstein et al. 2010) and limit II defined by $\Delta H^{*} = -11 \times \log(C^{*}_{298K}) + 85$ (Ranjan et al. 2012; Xie et al. 2025). As shown in Figure S9, the majority of ambient aerosol components tend to cluster closer to limit II. Based on those observations, this study adopts limit II semi-empirical parameterization for estimating the $^{i}\Delta H^{*}$ of plastic-derived thermal decomposition products. Consequently, the temperature-dependent $^{i}C^{*}_{T}$ values of species (i) are determined using the Clausius – Clapeyron Equation (6), using the parametrically derived values of $^{i}C^{*}_{298K}$ and $^{i}\Delta H^{*}$.

$$C^{*}_{T} = C^{*}_{298K}\left(\frac{298K}{T}\right)\exp\left[-\frac{^{i}\Delta H^{*}}{R}\left(\frac{1}{T}-\frac{1}{298K}\right)\right] \quad (6)$$

The temperature-dependent VBS distributions of the detected plastic thermal decomposition products are then constructed by grouping individual species into a series of bins (j), defined by integer values of $(\log C^{*})_{j}$. The corresponding temperature-dependent relative heights ($H_{T,j}$) of each VBS bin are then calculated using Equation (7):

$$H_{T,j} = \frac{\left[\sum_i f_i {}^{i}C^{*}_{T}\right]_j}{\sum_j\left[\sum_i f_i {}^{i}C^{*}_{T}\right]_j} \text{ where } \sum_j H_{T,j} = 1 \quad (7)$$

The particle-phase mass fractions of plastic thermal decomposition products, if aerosolized at given total organic mass (tOM) loading and temperature (T) in the air (C_{tOM}, μg·m^{-3}), can be calculated for each volatility bin (j) using Equation (8).

$$X^{p}_{T,j} = H_{T,j} \times \frac{C_{tOM}}{C_{tOM} + \left[\sum_i {}^{i}C^{*}_{T}\right]_j} \quad (8)$$

Overall, the methodology described above and summarized in Figure 2 enables the construction of VBS distributions for mixtures of plastic thermal decomposition products across a range of atmospherically relevant temperatures (T). It also facilitates the estimation of their equilibrium gas-phase and particle-phase fractions under varying tOM loading conditions.

To evaluate the effects of emissions from WUI fires involving both biomass and plastic-derived components, the VBS distributions derived for plastic thermal decomposition products can be numerically combined with VBS profiles for other WUI-relevant emission components, such as those previously reported for BBOA (Xie et al. 2024a). This approach enables the construction of representative VBS distributions for mixed-source emissions. Specifically, a composite VBS distribution for emissions from N distinct sources, each characterized by its own VBS profile, can be calculated using Equation (9).

$$H^{\Sigma N}_{T,j} = \frac{\sum_N x^{N} H^{N}_{T,j}}{\sum_j\left[\sum_N x^{N} H^{N}_{T,j}\right]_j} \quad (9)$$

Here, $H^{\Sigma N}_{T,j}$ represents the temperature-dependent height of the volatility bin (j) constructed for a mixture containing N components, each contributing a mass fraction x^{N} (Σx^{N}=1). As an approximation, these x^{N} values can be used to represent the relative contributions of various fuel types considered for WUI emissions. Figure 3 presents a numerically constructed VBS distribution for a hypothetical emission mixture composed of 50% biomass burning organic aerosol (BBOA) and 50% polypropylene (PP), which was thermally decomposed and then cooled to $T = 50\,^{\circ}C$ and $C_{tOM} = 100\,\mu g/m^{3}$. The accompanying pie charts illustrate the fractions of each emission source that would partition between the gas- and particle-phase under these conditions. This composite VBS framework enables the numeric evaluation of how mixed emission sources influence overall gas–particle partitioning behavior. For example, under the specified T and

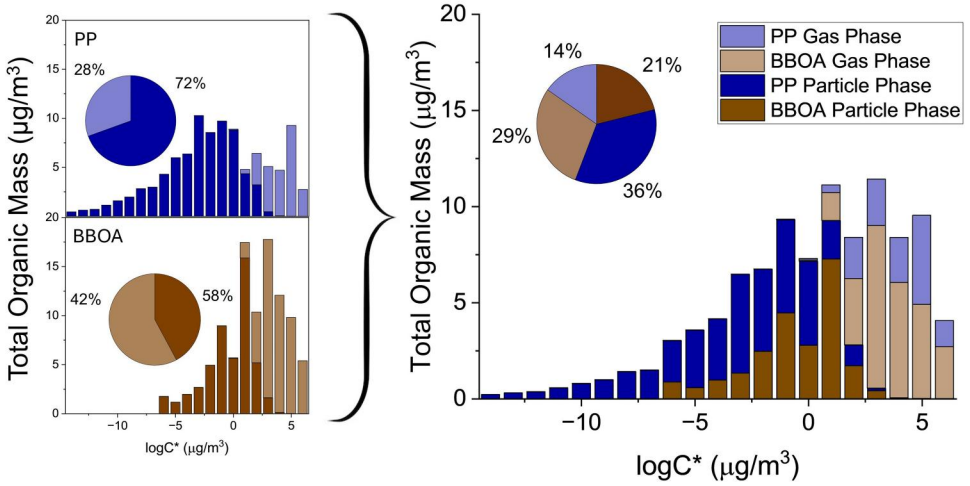

Figure 3. Numerically constructed VBS distribution representing an emission mixture composed of 50% biomass burning organic aerosol (BBOA) and 50% polypropylene (PP) thermal decomposition products calculated at $T = 50\,^{\circ}C$ and $C_{tOM} = 100\,\mu g/m^3$.

C_{tOM} conditions, burning of a 50/50 mixture of PP and biomass fuel would produce an aerosol with lower volatility and a greater particle-phase fraction compared to biomass emissions alone. This shift in partitioning has direct implications for the chemical reactivity, optical properties, and contribution to $PM_{2.5}$ mass of the resulting aerosol mixture.

Chemical variability of plastic thermal decomposition products. The thermal decomposition products of common plastic materials exhibit significant variability in both molecular size and compositional distribution. Figure 4 presents the mass spectra of plastic thermal decomposition products determined in TPD-(+)DART-HRMS experiments for four major plastic types: PP, PE, PS, and PVC. The background colors delineate approximate regions of volatility classes with minor variations from differences in molecular formula, including volatile organic compounds (VOC), intermediate volatile organic compounds (IVOC), semi-volatile organic compounds (SVOC), low volatile organic compounds (LVOC), and extremely low volatility organic compounds (ELVOC), previously defined in Donahue et al. (2012) to describe the volatility of organic compounds. The individual formula assignments and chemical properties of the species identified for each plastic type are discussed in detail in Halpern et al. (2025). The results demonstrate that each plastic generates a distinct spectrum of thermal decomposition products, leading to aerosol emissions with differing volatility profiles. Specifically, PP and PE produce a broad distribution of species spanning the full volatility range from VOC to ELVOC, with a significant proportion of compounds falling within LVOC and ELVOC categories. PS products are characterized by a distinct region of larger, lower volatility species, along with a significant cluster of abundant species falling in the IVOC category. PVC products exhibit a comparatively narrower range of volatility classes, with minimal contribution from ELVOC species. The corresponding mass spectra obtained in TPD-(−)DART-HRMS experiments are provided in Figure S10. Overall, Figures 4 and S10 highlight the substantial variability in the chemical composition and volatility of plastic thermal decomposition products, which directly influence the physicochemical properties of aerosols emitted by WUI fires.

Assessment of gas-particle partitioning in mixed emissions. The VBS distributions calculated across a wide range of temperatures and total organic mass loadings provide numerical values for constructing two-dimensional (2D) maps that depict the equilibrium gas-particle partitioning of aerosolized mixtures as a function of T and C_{tOM}. Figure 5 presents the 2D gas-particle partitioning maps for the thermal decomposition products of four plastic types investigated in this study (PP, PE, PS, and PVC). These maps visualize the differences in gas-particle partitioning behavior among the thermal decomposition products of these plastics and illustrate how they may evolve during atmospheric transport. The maps reveal that within concentrated plumes of WUI smoke emissions ($C_{tOM} > 100\,\mu g/m^3$), the majority of plastic-derived products are expected to reside in the particle phase (>80%) at relatively low ambient temperatures approaching 25 °C. This leads to higher particle counts, elevated concentrations of $PM_{2.5}$, and slower aging due to limited volatilization. Notably, under any combination of T and C_{tOM} conditions, the thermal decomposition products of PP exhibit greater preference for particle-phase (i.e., higher condensability) compared to those

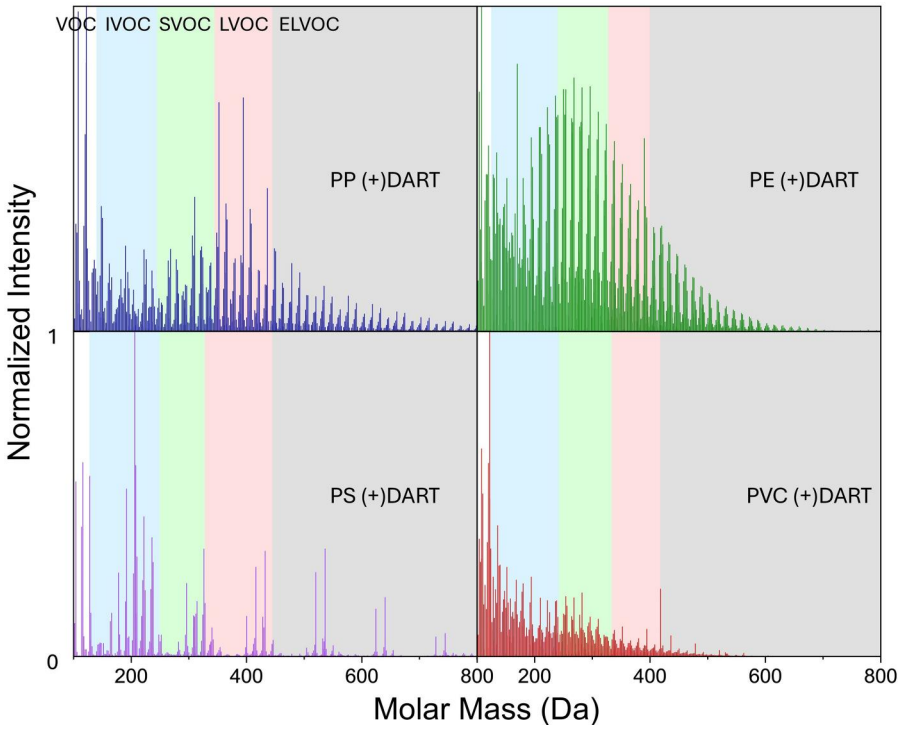

Figure 4. Mass spectra of thermal decomposition products obtained in TPD-(+)DART-HRMS experiments with four common plastic types: polypropylene (PP), polyethylene (PE), polystyrene (PS), and polyvinyl chloride (PVC). The background color regions indicate approximate volatility classes: volatile organic compounds (VOC), intermediately volatile organic compounds (IVOC), semi-volatile organic compounds (SVOC), low volatile organic compounds (LVOC), and extremely low volatility organic compounds (ELVOC).

from PE, PS, and PVC. This framework enables quantitative estimation of how the burning of different plastic types influences gas-particle partitioning in WUI emissions. The corresponding 2D maps derived from TPD-(−)DART-HRMS experiments are shown in Figure S11 and display similar trends to those in Figure 5.

Similar 2D gas-particle partitioning maps can be generated using numerically constructed VBS distributions representing hypothetical WUI fire emissions composed of products from mixed plastic and biomass fuels. Figure 6 illustrates one such example, showing the numerically estimated gas-particle partitioning behavior for an emission mixture containing 50% BBOA and 50% of PP thermal decomposition products. Under typical ambient temperatures (<40 °C), PP-derived products are predicted to be more condensable than those from BBOA, with over 70% of their mass residing in the particle phase. When PP plastic fuel is co-burned with biomass, the resulting emission mixture is expected to exhibit condensability between BBOA and PP. This framework also enables a detailed assessment of how gas–particle partitioning evolves under atmospheric conditions typically encountered by WUI fire plumes. As the emissions move away from the source, they undergo both cooling and dilution, leading to dynamic changes in the extent of gas-particle partitioning of their components. In Figure 6, the trajectory along points 1–5 represents initial cooling of the plume, followed by dilution along trajectory points 5–9, representing a hypothetical series of conditions for a mixed WUI fire emission. For each of these trajectory points, associated gas- and particle-phase mass loadings can be extracted (Table S1), along with their corresponding VBS distributions, providing practical data for atmospheric modeling of plume evolution, which can be used for atmospheric modeling studies. Additional 2D gas-particle partitioning maps for 50/50 emission mixtures of BBOA with thermal decomposition products from PE, PS, and PVC are included in Figure S12.

Figure 7 presents the estimated particle-phase fractions for mixed emissions composed of BBOA with plastic thermal decomposition products derived from each of the four plastic types (PP, PE, PS, and PVC), evaluated at mixing ratios of 0% (all BBOA), 10%, 25%, and 50%. Calculations are performed along the same trajectory points (1–9) defined in Figure 6 and detailed in Table S1. The results indicate that the addition of plastic-derived products has a minimal impact on gas-particle partitioning at high mass loadings and elevated temperatures (point 1). However, as the plume cools down and dilutes during atmospheric transport, the presence of plastic thermal degradation

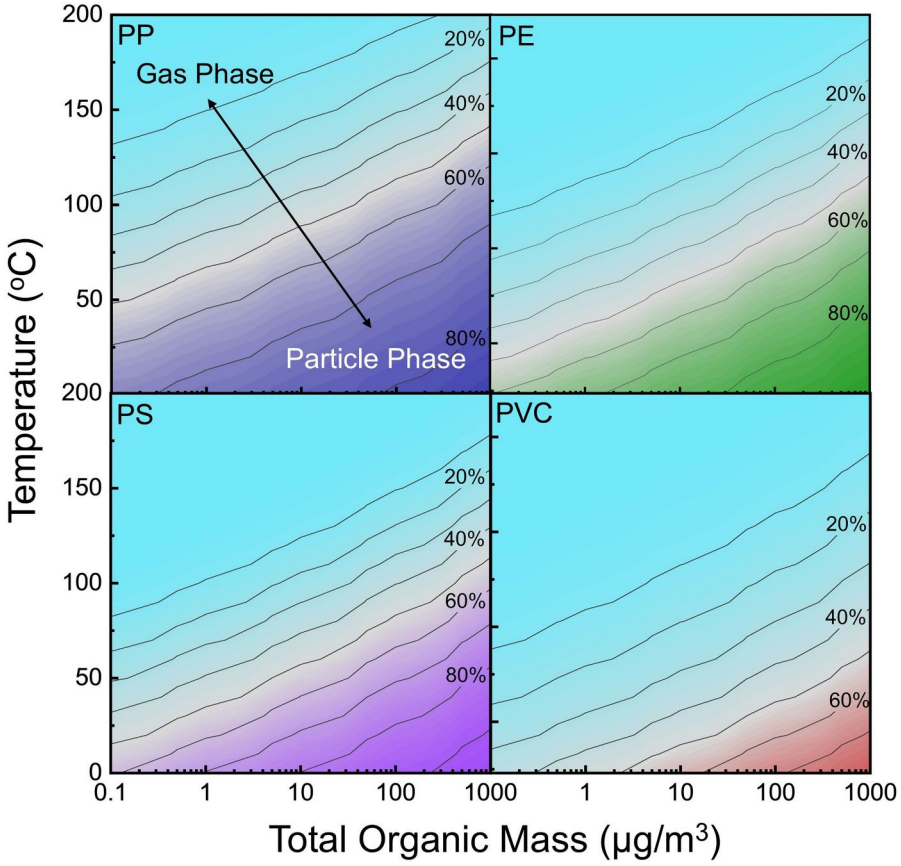

Figure 5. 2D gas-particle partitioning maps for thermal decomposition products of four plastic types (PE, PP, PS, and PVC) calculated from VBS distributions derived using TPD-(+)DART-HRMS experiments. Each map depicts the equilibrium partitioning behavior of plastic-derived products across a broad range of ambient temperatures and total organic mass loadings, illustrating the relative propensity of each plastic's pyrolysis products to exist in the particle versus gas phase under atmospherically relevant conditions.

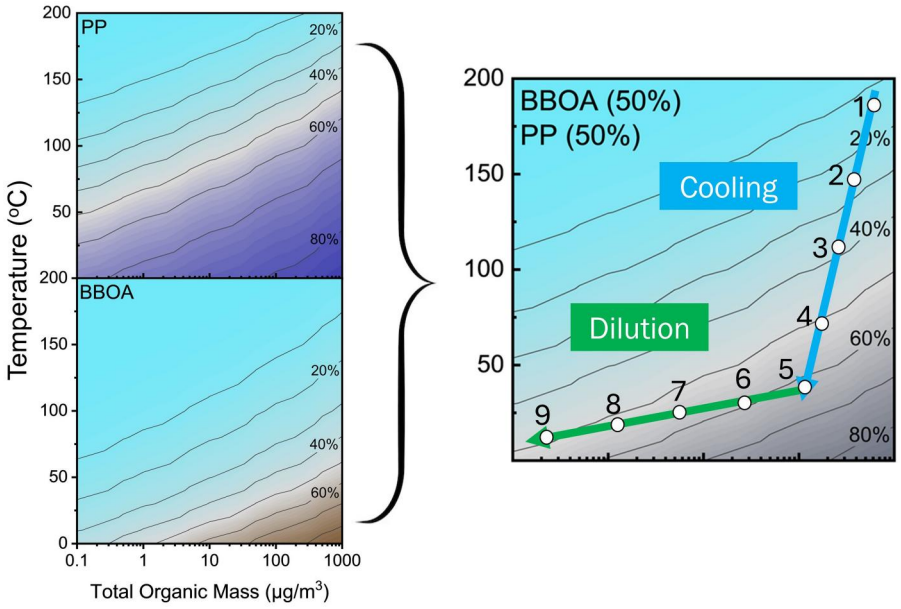

Figure 6. 2D gas-particle maps of BBOA and PP-derived thermal decomposition products (left panels), along with a composite map representing a 50/50 mixed emission from BBOA and PP products (right panel). The trajectories along points 1–9 illustrate an example of cooling (points 1–5) and dilution (points 5–9) experienced by fire emissions as they disperse from the source.

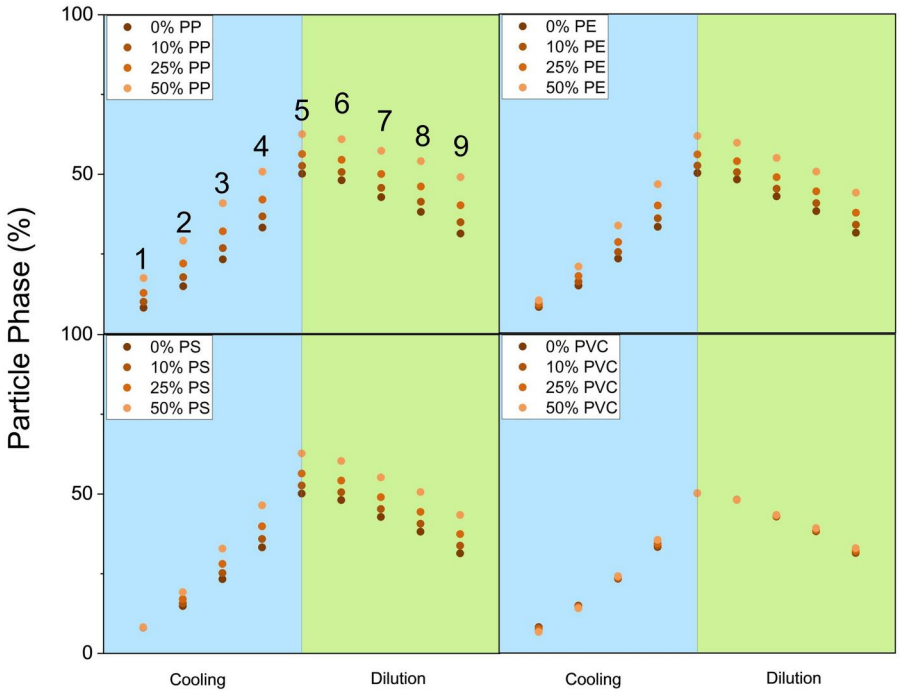

Figure 7. Particle-phase fractions of mixed emissions composed of BBOA and thermal decomposition products derived from four plastic types (PP, PE, PS, and PVC) at mixing ratios of 0% (all BBOA), 10%, 25%, and 50%. Calculations are performed for T and C_{tOM} conditions corresponding to trajectory points 1–9, as depicted in Figure 6, illustrating an example of emissions evolution through cooling (points 1–5) and dilution (points 5–9) as the plume disperses from the source.

products leads to a more substantial increase in the particle-phase fraction (point 9), particularly at higher plastic contributions (≥25%). While the thermal decomposition products of PE, PP, and PS exhibit a similar qualitative effect on the resulting mixed emissions after their atmospheric cooling and dilution, their expected quantitative impacts vary by plastic type. Specifically, PP-derived products exhibit the most significant influence on the formation of condensed phase species, resulting in higher particle-phase fractions upon cooling and dilution. PS- and PE-derived products exhibit a moderate effect, with lower particle-phase formation compared to PP. PVC-derived products have the least impact on the gas–particle partitioning of the emission plume, reflecting their lower tendency to condense into the particle phase. These results underscore the importance of plastic type in determining the atmospheric behavior of mixed WUI fire emissions.

Viscosity estimates of mixed emission particles. The explicit data on the particle-phase composition obtained from our measurements also enables the prediction of glass transition temperatures (T_g) and, subsequently, the viscosity of particle-phase dry mixtures at various T and C_{tOM} conditions. Details of the viscosity estimates for single-emission-source aerosols are provided in Supplemental Note 5. To extend these calculations to mixed emissions composed of N sources, the combined T_g of the mixture can be estimated using a weighted average approach:

$$T_{g,\mathrm{mix}} = \left(\sum\nolimits_N x^N T_g^N\right) \tag{10}$$

where T_g^N is the class transition temperature of the particle-phase mixture derived from source N, and $x^N (\Sigma x^N = 1)$ is its mass fraction in the composite mixture.

The viscosity of this composite mixture can then be calculated under varying relative humidity (RH) conditions. Mixtures of plastic thermal decomposition products are predicted to exhibit a wide range of viscosities depending on the plastic type, as illustrated in Figure S13. Emissions of PE- and PP-derived products are estimated to form particles with substantially higher viscosity than BBOA (Figure S14), whereas PS- and PVC-derived products are predicted to form particles with relatively lower viscosity comparable to that of BBOA. The approach presented in this study enables estimation of viscosity for particle-phase mixtures containing composite products, such as those formed from combined BBOA and plastic thermal decomposition products. Figure 8 illustrates the predicted viscosities of such mixtures as a function of RH, assuming a hygroscopicity parameter (κ) of 0.1, representative of BBOA-like materials (Petters and

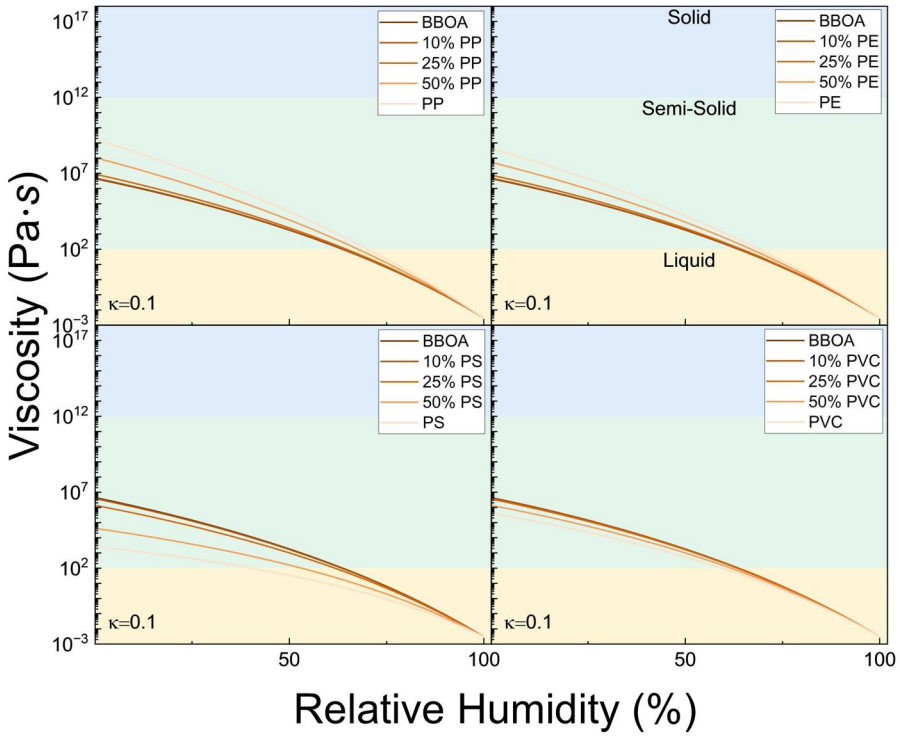

Figure 8. Viscosity of composite particles composed of BBOA and thermal decomposition products derived from four plastic types (PP, PE, PS, and PVC) at mixing ratios of 0% (all BBOA), 10%, 25%, 50%, and 100% (all plastic-derived products). Viscosity values at dry conditions (0% RH) were calculated under conditions of C_{tOM} =100 μg/m^3 and 25 °C. Humidity-dependent values were calculated assuming a hygroscopicity parameter $\kappa = 0.1$. Additional plots, assuming lower κ values of 0.05 and 0.02, are provided in Figures S15 and S16.

Kreidenweis 2007). Additional viscosity plots containing estimates using κ values of 0.02 and 0.05 are provided in Figures S15 and S16. These viscosity values can also be determined for mixtures at different temperatures, as shown in Figure S17. Mixtures containing PP- and PE-derived products are predicted to substantially increase the viscosity of the aerosol particles, whereas PS- and PVC-derived products may reduce viscosity when mixed with BBOA. For example, PP-derived products contribute to a 100-fold increase in viscosity at a 50% mixing ratio and 0% RH, shifting the particle phase from semi-solid to solid (DeRieux et al. 2018). In contrast, a 50% contribution of PS-derived products under the same conditions reduces the viscosity of the composite particles from 10^{11} Pa·s to 10^{7} Pa·s, significantly increasing the permeability of the particles. Interestingly, although PE- and PS-derived products have comparable effects on gas-particle partitioning in their corresponding composite mixtures (Figure 7), they produce opposite viscosity trends. The addition of PE products increases the viscosity of the composite mixture, while the addition of PS products decreases the viscosity when mixed with BBOA. This effect is attributed to significant differences in the molecular metrics of PE- and PS-derived products, such as their oxygen content and aromaticity (Figure S2-S4). The ability to predict viscosity is critical, as it governs internal mixing times, diffusion rates, and chemical reactivity in the atmosphere. These findings underscore the strong influence of plastic type on aerosol phase behavior and highlight the importance of this methodology for evaluating the environmental implications of WUI fire emissions containing plastic materials.

Conclusions and outlook

The approach presented in this study provides a quantitative framework for estimating both gas-particle partitioning and viscosity of atmospheric particles representative of WUI fire emissions. By integrating TPD-DART-HRMS experimental datasets describing the molecular composition of thermal decomposition products of representative plastic with the VBS method, this approach enables practical evaluation of mixed emission properties, offering critical input for environmental modeling of aerosol behavior. This framework is particularly useful for predicting WUI fire emissions, where aerosol composition and phase distribution are influenced by a wide

range of factors, including fuel heterogeneity, combustion conditions, and atmospheric variability. All estimates reported in this work utilized the limit II of the ΔH^* versus $\log(C^*_{298K})$ correlation (Ranjan et al. 2012). Alternative values calculated using the limit I correlation are provided in Supplementary Note 6 and Figures S18–S20, indicating similar qualitative trends. The real-world volatility characteristics of plastic thermal decomposition mixtures require further investigation to more accurately constrain the gas-particle partitioning behavior of mixed aerosol emissions. It is likely that additional chemical and physical processes, such as multi-phase reactions between species from different sources, combustion dynamics in large-scale fires, and variable environmental conditions, influence both gas-particle partitioning and aerosol viscosity in ways not captured by the presented numerical framework. Consequently, future work is needed to validate and refine these estimates through direct experimental measurements of volatility and phase behavior of ambient WUI aerosol mixtures. The numerical estimation approach presented here offers a scalable solution to the inherent complexity of WUI aerosol mixtures, especially those involving plastic thermal decomposition products, which vary significantly with polymer type and heating conditions (Bockhorn et al. 1999; Wu et al. 2021). Direct experimental characterization of all possible emission combinations is impractical, making this modeling approach a valuable alternative. In addition to predicting gas–particle partitioning, this methodology allows estimation of aerosol viscosity and particle-phase mixing times, which are essential for assessing the chemical reactivity and transformation of WUI-derived aerosols. These properties directly impact key atmospheric processes such as chemical aging, secondary organic aerosol formation, and cloud condensation or ice nucleation activity. As such, the framework developed in this work provides a practical tool for advancing our understanding of the environmental and air quality impacts of complex WUI fire emissions.

These estimates can be directly applied to improve environmental modeling of multi-component emissions from WUI fires. Additionally, the TPD-DART-HRMS-derived volatility estimates are adaptable to a wide range of emission sources. For example, volatility characteristics of biogenic secondary organic aerosols (West et al. 2023; Xie et al. 2024b) can be combined with those of plastic thermal decomposition products or BBOA to model gas-particle partitioning in other mixed emission scenarios. This approach can also be extended to other aerosol types, including anthropogenic urban emissions (Xie et al. 2025b). Moreover, the method is well-suited for evaluating a broader range of emissions relevant to degradation products from other plastic materials, including waste, aged, and recycled plastics, enabling investigation into how contamination and environmental aging alter the chemical composition and gas–particle partitioning behavior of their thermal decomposition products.

Author contributions

E.H. and A.L. designed the study. E.H. conducted experiments assisted by P.C, K.M, and L.H., D.D. performed Q-Chem 5 calculations. Q.X., P.C., K.M. and L.H. assisted in data acquisition and data analysis. E.H. and A.L. wrote the manuscript with contributions from all coauthors. A.L. and S.N. secured grant funding for this study and directed the overall project.

Disclosure statement

No potential conflict of interest was reported by the author(s).

Funding

This work was supported by the National Oceanic and Atmospheric Administration grants NA22OAR4310195 (Purdue University) and NA22OAR4310196 (University of California, Irvine). E.H. acknowledges support from the Bilsland Dissertation Fellowship provided by the Department of Chemistry and the Graduate School of Purdue University.

ORCID

Emily Halpern http://orcid.org/0000-0003-2009-6807
Dominick Dotson http://orcid.org/0009-0007-7506-7700
Qiaorong Xie http://orcid.org/0000-0002-9391-624X
Peter Christ http://orcid.org/0000-0002-6025-7073
Sergey A. Nizkorodov http://orcid.org/0000-0003-0891-0052
Alexander Laskin http://orcid.org/0000-0002-7836-8417

References

Balch JK et al. 2017. Human-started wildfires expand the fire niche across the United States. Proc Natl Acad Sci USA. 114(11):2946–2951. https://doi.org/10.1073/pnas.1617394114

Bardales Cruz M et al. 2023. Plastic waste generation and emissions from the domestic open burning of plastic waste in Guatemala. Environ Sci Atmos. 3(1):156–167. https://doi.org/10.1039/d2ea00082b

Benedict K et al. 2024. Wildland urban interface (WUI) Emissions: laboratory measurement of aerosol and trace gas from combustion of manufactured building materials. ACS EST Air. 1(12):1673–1686. https://doi.org/10.1021/acsestair.4c00217

Bockhorn H, Hornung A, Hornung U. 1999. Mechanisms and kinetics of thermal decomposition of plastics from isothermal and dynamic measurements. J Anal Appl Pyrolysis. 50(2):77–101. https://doi.org/10.1016/S0165-2370(99)00026-1

Burke M et al. 2023. The contribution of wildfire to PM2.5 trends in the USA. Nature. 622(7984):761–766.): https://doi.org/10.1038/s41586-023-06522-6

Chakrabarty RK et al. 2023. Shortwave absorption by wildfire smoke dominated by dark brown carbon. Nat Geosci. 16(8):683–688. https://doi.org/10.1038/s41561-023-01237-9

Chernetsova ES, Morlock GE, Revelsky IA. 2011. DART mass spectrometry and its applications in chemical analysis. Russ Chem Rev. 80(3):235–255. https://doi.org/10.1070/RC2011v080n03ABEH004194

DeRieux WSW et al. 2018. Predicting the glass transition temperature and viscosity of secondary organic material using molecular composition. Atmos Chem Phys. 18(9):6331–6351. https://doi.org/10.5194/acp-18-6331-2018

Donahue NM, Epstein SA, Pandis SN, Robinson AL. 2011. A two-dimensional volatility basis set: 1. organic-aerosol mixing thermodynamics. Atmos Chem Phys. 11(7):3303–3318. https://doi.org/10.5194/acp-11-3303-2011

Donahue NM, Kroll JH, Pandis SN, Robinson AL. 2012. A two-dimensional volatility basis set – part 2: diagnostics of organic-aerosol evolution. Atmos Chem Phys. 12(2):615–634. https://doi.org/10.5194/acp-12-615-2012

Epifanovsky E et al. 2021. Software for the frontiers of quantum chemistry: an overview of developments in the Q-Chem 5 package. J Chem Phys. 155(8):084801. https://doi.org/10.1063/5.0055522

Epstein SA, Riipinen I, Donahue NM. 2010. A Semiempirical correlation between enthalpy of vaporization and saturation concentration for organic aerosol. Environ Sci Technol. 44(2):743–748. https://doi.org/10.1021/es902497z

Fang T et al. 2023. Wildfire particulate matter as a source of environmentally persistent free radicals and reactive oxygen species. Environ Sci Atmos. 3(3):581–594. https://doi.org/10.1039/D2EA00170E

Fang Z et al. 2025. Investigating the oxidative potential and in vitro toxicity of ambient water-soluble PM10 in an eastern Mediterranean site. ACS EST Air. 2(7):1326–1338. https://doi.org/10.1021/acsestair.5c00085

Forbes TP, Pettibone JM, Windsor E, Conny JM, Fletcher RA. 2023. Rapid chemical screening of microplastics and nanoplastics by thermal desorption and pyrolysis mass spectrometry with unsupervised fuzzy clustering. Anal Chem. 95(33):12373–12382. https://doi.org/10.1021/acs.analchem.3c01897

Ganteaume A, Barbero R, Jappiot M, Maillé E. 2021. Understanding future changes to fires in southern Europe and their impacts on the wildland-urban interface. J Safety Sci Resilience. 2(1):20–29. https://doi.org/10.1016/j.jnlssr.2021.01.001

Gonçalves CK, Tenório JAS, Levendis YA, Carlson JB. 2008. Emissions from premixed combustion of polystyrene. Energy Fuels. 22(1):354–362. https://doi.org/10.1021/ef700431f

Gross JH. 2014. Direct analysis in real time-a critical review on DART-MS. Anal Bioanal Chem. 406(1):63–80. https://doi.org/10.1007/s00216-013-7316-0

Halpern E et al. 2025. Chemical characterization of polymer and chloride content in waste plastic materials using pyrolysis – direct analysis in real time – high-resolution mass spectrometry. Environ Sci Process Impacts. 27(1):104–118. https://doi.org/10.1039/D4EM00501E

Hammer, R.B., Stewart, S.I., and Radeloff, V.C. (2009). Demographic trends, the wildland-urban interface, and wildfire management. Soc Nat Resources. 22(8):777–782. https://doi.org/10.1080/08941920802714042

Hoffer A et al. 2020. Emission factors for PM_{10} and polycyclic aromatic hydrocarbons (PAHs) from illegal burning of different types of municipal waste in households. Atmos Chem Phys. 20(24):16135–16144. https://doi.org/10.5194/acp-20-16135-2020

Holder AL, Ahmed A, Vukovich JM, Rao V. 2023. Hazardous air pollutant emissions estimates from wildfires in the wildland urban interface. PNAS Nexus. 2(6):pgad186. https://doi.org/10.1093/pnasnexus/pgad186

Hopstock KS et al. 2024. Molecular characterization and photoreactivity of organic aerosols formed from pyrolysis of urban materials during fires at the wildland–urban interface. ACS EST Air. 1(11):1495–1506. https://doi.org/10.1021/acsestair.4c00215

Huang J et al. 2018. Thermal decomposition mechanisms of poly(vinyl chloride): a computational study. Waste Manag. 76:483–496. https://doi.org/10.1016/j.wasman.2018.03.033

Hughey CA, Hendrickson CL, Rodgers RP, Marshall AG. 2001. Elemental composition analysis of processed and unprocessed diesel fuel by electrospray ionization Fourier transform ion cyclotron resonance mass spectrometry. Energy Fuels. 15(5):1186–1193. https://doi.org/10.1021/ef010028b

Jaffe DA et al. 2020. Wildfire and prescribed burning impacts on air quality in the United States. J Air Waste Manag Assoc. 70(6):583–615. https://doi.org/10.1080/10962247.2020.1749731

Jaitly N et al. 2009. Decon2LS: An open-source software package for automated processing and visualization of high resolution mass spectrometry data. BMC Bioinformatics. 10(87):1–15. https://doi.org/10.1186/1471-2105-10-87

Koch BP, Dittmar T. 2006. From mass to structure: an aromaticity index for high-resolution mass data of natural organic matter. Rapid Comm Mass Spectrometry. 20(5):926–932. https://doi.org/10.1002/rcm.2386

Kroll JH et al. 2011. Carbon oxidation state as a metric for describing the chemistry of atmospheric organic aerosol. Nat Chem. 3(2):133–139. https://doi.org/10.1038/nchem.948

Laskin A, Laskin J, Nizkorodov SA. 2015. Chemistry of atmospheric brown carbon. Chem Rev. 115(10):4335–4382. https://doi.org/10.1021/cr5006167

Laskin A, West CP, Hettiyadura APS. 2025. Molecular insights into the composition, sources, and aging of atmospheric brown carbon. Chem Soc Rev. 54(3):1583–1612. https://doi.org/10.1039/D3CS00609C

Li Y, Pöschl U, Shiraiwa M. 2016. Molecular corridors and parameterizations of volatility in the chemical evolution of organic aerosols. Atmos Chem Phys. 16(5):3327–3344. https://doi.org/10.5194/acp-16-3327-2016

Liang Y et al. 2023. Gas–particle partitioning of semivolatile organic compounds when wildfire smoke comes to town.

Atmos Chem Phys. 23(19):12441–12454. https://doi.org/10.5194/acp-23-12441-2023

Meija J. 2006. Mathematical tools in analytical mass spectrometry. Anal Bioanal Chem. 385(3):486–499. https://doi.org/10.1007/s00216-006-0298-4

Murphy BN et al. 2012. Functionalization and fragmentation during ambient organic aerosol aging: application of the 2-D volatility basis set to field studies. Atmos Chem Phys. 12(22):10797–10816. https://doi.org/10.5194/acp-12-10797-2012

National Academies of Sciences, Engineering, and Medicine; Division on Earth and Life Studies; Board on Chemical Sciences and Technology; Committee on the Chemistry of Urban Wildfires. 2022. The chemistry of fires at the wildland-urban interface. The National Academies Press.

Petters MD, Kreidenweis SM. 2007. A single parameter representation of hygroscopic growth and cloud condensation nucleus activity. Atmos Chem Phys. 7(8):1961–1971. https://doi.org/10.5194/acp-7-1961-2007

Ranjan M, Presto AA, May AA, Robinson AL. 2012. Temperature dependence of gas–particle partitioning of primary organic aerosol emissions from a small diesel engine. Aerosol Sci Technol. 46(1):13–21. https://doi.org/10.1080/02786826.2011.602761

Roach PJ, Laskin J, Laskin A. 2011. Higher-order mass defect analysis for mass spectra of complex organic mixtures. Anal Chem. 83(12):4924–4929. https://doi.org/10.1021/ac200654j

Salim R et al. 2025. Plastic burning particulate matter as a source of environmentally persistent free radicals and reactive oxygen and chlorine species. npj Clean Air. 1(1):14. https://doi.org/10.1038/s44407-025-00015-8

Shrivastav V, Nahin M, Hogan CJ, Larriba-Andaluz C. 2017. Benchmark comparison for a multi-processing ion mobility calculator in the free molecular regime. J Am Soc Mass Spectrom. 28(8):1540–1551. https://doi.org/10.1007/s13361-017-1661-8

West CP et al. 2023. Volatility measurements of individual components in organic aerosol mixtures using temperature-programmed desorption–direct analysis in real time–high resolution mass spectrometry. Anal Chem. 95(19):7403–7408. https://doi.org/10.1021/acs.analchem.3c00923

Wu D et al. 2021. Commodity plastic burning as a source of inhaled toxic aerosols. J Hazard Mater. 416:125820. https://doi.org/10.1016/j.jhazmat.2021.125820

Xie Q et al. 2024a. Molecular insights into gas–particle partitioning and viscosity of atmospheric brown carbon. Environ Sci Technol. 58(41):18284–18294. https://doi.org/10.1021/acs.est.4c05650

Xie Q et al. 2024b. Volatility basis set distributions and viscosity of organic aerosol mixtures: insights from chemical characterization using temperature-programmed desorption–direct analysis in real-time high-resolution mass spectrometry. Anal Chem. 96(23):9524–9534. https://doi.org/10.1021/acs.analchem.4c01003

Xie Q et al. 2025. Molecular characterization of composition and volatility of ambient organic aerosol sampled by an UAV-mounted portable aethalometer. Anal Chem. 97(32):17743–17751. https://doi.org/10.1021/acs.analchem.5c03027

Zhang J et al. 2023. Bulk and molecular-level composition of primary organic aerosol from wood, straw, cow dung, and plastic burning. Atmos Chem Phys. 23(22):14561–14576. https://doi.org/10.5194/acp-23-14561-2023

Zhang X et al. 2020. Rapid Monitoring approach for microplastics using portable pyrolysis-mass spectrometry. Anal Chem. 92(6):4656–4662. https://doi.org/10.1021/acs.analchem.0c00300